Title

Kinesins relocalize the chromosomal passenger complex to the midzone for spindle disassembly.

Journal

The Journal of cell biology, 217(5)

ISSN

0021-9525

Authors

Ibarlucea-Benitez, Itziar
Ferro, Luke S
Drubin, David G
et al.

Publication Date

2018-05-01

DOI

10.1083/jcb.201708114

Peer reviewed

JCB Journal of Cell Biology

ARTICLE

Kinesins relocalize the chromosomal passenger complex to the midzone for spindle disassembly

Itziar Ibarlucea-Benitez[1], Luke S. Ferro[2], David G. Drubin[2], and Georjana Barnes[2]

Mitotic spindle disassembly after chromosome separation is as important as spindle assembly, yet the molecular mechanisms for spindle disassembly are unclear. In this study, we investigated how the chromosomal passenger complex (CPC), which contains the Aurora B kinase Ipl1, swiftly concentrates at the spindle midzone in late anaphase, and we researched the role of this dramatic relocalization during spindle disassembly. We showed that the kinesins Kip1 and Kip3 are essential for CPC relocalization. In cells lacking Kip1 and Kip3, spindle disassembly is severely delayed until after contraction of the cytokinetic ring. Purified Kip1 and Kip3 interact directly with the CPC and recruit it to microtubules in vitro, and single-molecule experiments showed that the CPC diffuses dynamically on microtubules but that diffusion stops when the CPC encounters a Kip1 molecule. We propose that Kip1 and Kip3 trap the CPC at the spindle midzone in late anaphase to ensure timely spindle disassembly.

Introduction

The Aurora B kinase (Ipl1 in budding yeast) is part of the chromosomal passenger complex (CPC), which associates with chromosomes and the mitotic spindle and is one of the master regulators of mitosis (Shannon and Salmon, 2002; Nakajima et al., 2009). The CPC is conserved across eukaryotes and has a very dynamic localization throughout mitosis, which allows it to regulate different spindle components during different stages of this process (Petersen et al., 2001; Murata-Hori et al., 2002). Targets of the CPC include several microtubule-associated proteins that regulate the intrinsic dynamic behavior of microtubules to orchestrate the different stages of mitosis and ensure the fidelity of chromosome segregation (Hsu et al., 2000; Cheeseman et al., 2002; Kotwaliwale et al., 2007; Zimniak et al., 2009; Woodruff et al., 2010). One subgroup of microtubule-associated proteins of particular relevance to this study localizes at the spindle midzone, where microtubule plus ends extending from two spindle poles overlap. These proteins include both motor and nonmotor proteins. Their functions at the midzone are mainly to stabilize the overlapping region of antiparallel microtubules (e.g., Bim1, the budding yeast homologue of EB1, and Ase1, budding yeast PRC1) and to drive spindle assembly by promoting plus end microtubule assembly and generating an outwardly directed force (e.g., the kinesin 5 motors Kip1 and Cin8) that pushes the microtubule organizing centers (spindle pole bodies in yeast) apart (Saunders and Hoyt, 1992). Roles for these proteins at the end of mitosis are poorly understood.

In late anaphase, the CPC is known to regulate two processes. The first is spindle disassembly, which it regulates in part by phosphorylating and inactivating the microtubule-stabilizing protein Bim1, leading to its dissociation from the midzone and hence spindle destabilization (Buvelot et al., 2003; Zimniak et al., 2009). Ipl1 phosphorylation of the microtubule-destabilizing protein She1 is also important for efficient spindle disassembly (Woodruff et al., 2010). Another process regulated by the CPC is the NoCut pathway, a checkpoint that ensures that chromosomes have cleared the plane of division before cytokinesis starts (Norden et al., 2006).

Just before the onset of spindle disassembly, the CPC dramatically changes its localization from being evenly distributed along the entire length of the spindle to being concentrated at the midzone, where it presumably acts to promote spindle disassembly and mitotic exit. This relocalization is swift and not well understood. A possible mechanism could be that the CPC gets transported to the midzone by a plus end–directed kinesin because the spindle midzone is formed by overlapping microtubule plus ends that emanate from opposite poles. Alternatively, the CPC might diffuse on the microtubules and get trapped at the spindle midzone through interaction with midzone proteins and/or overlapping microtubule ends. Another possible scenario is

[1]Biophysics Graduate Group, University of California, Berkeley, Berkeley, CA; [2]Department of Molecular and Cell Biology, University of California, Berkeley, Berkeley, CA.

Correspondence to Georjana Barnes: gbarnes@berkeley.edu.

https://doi.org/10.1083/jcb.201708114

that soluble CPC from the cytosol is captured at the midzone by a midzone protein. From research on mammalian cells, we know that the kinesin 6 Mklp2 is required for CPC midzone localization (Gruneberg et al., 2004). However, despite the importance and highly conserved nature of this relocalization, whether it happens through direct interaction or an indirect mechanism is not known, nor is the functional importance of the relocalization understood. In budding yeast, there are only four nuclear kinesins: Cin8, Kip1, Kip3, and Kar3, and none of them belongs to the kinesin 6 family. Only the first three kinesins are plus end directed and as such would be good candidates to recruit the CPC to the central spindle.

Spindle disassembly is an essential process (Woodruff et al., 2012). However, very little is known about how it is regulated. In this study, we combined genetics, live-cell microscopy, biochemistry, and single-molecule fluorescence microscopy to investigate the role of the CPC during spindle disassembly. We describe the role of the different nuclear kinesins in this process and propose a mechanistic model for how the CPC gets targeted to the spindle midzone to promote spindle disassembly.

Results

The CPC colocalizes with Cin8, Kip1, and Kip3 at the spindle midzone during late anaphase

To determine whether any of the three plus end–directed nuclear kinesins might recruit the CPC to the midzone, we examined the localization of each motor and the CPC during late anaphase. We labeled the Nbl1 subunit of the CPC with an mCherry tag and combined it with GFP-labeled Cin8, Kip1, or Kip3 to look for colocalization. Nbl1-mCherry localizes all along the spindle early in anaphase and concentrates at the spindle midzone as the cell progresses through anaphase (Buvelot et al., 2003). In late anaphase, just before the onset of spindle disassembly, Nbl1-mCherry is found as a bright focus at the spindle midzone; once the spindle breaks, Nbl1-mCherry tracks the ends of shrinking spindle microtubules (Figs. 1 and S1; Nakajima et al., 2009). Avunie-Masala et al. (2011) reported that Cin8-GFP binds to microtubules in a wide region around the spindle midzone and at the poles, and as the spindle further elongates, the amount of Cin8-GFP at the midzone decreases. In cells undergoing late anaphase, we observed that some Cin8 localizes to the spindle midzone, colocalizing with Nbl1 throughout late anaphase (Fig. 1 A). Just before the onset of spindle disassembly, their peak fluorescence along the spindle aligns at the spindle midzone (Fig. 1 B). In agreement with previous research from Fridman et al. (2013), we observed that Kip1-GFP is located at the midzone during late anaphase and tracks microtubule plus ends upon spindle breakage (Fig. 1 C). Kip1 and Nbl1 colocalized throughout anaphase, and their fluorescence intensity peaks aligned at the spindle midzone just before the onset of spindle disassembly (Fig. 1 D). Similarly, Kip3 also colocalizes with Nbl1 at the spindle midzone in late anaphase (Fig. 1, E and F). Collectively, colocalization analysis showed that all three plus end–directed nuclear kinesins localize at the spindle midzone together with the CPC during late anaphase and are therefore candidates to target it to that region.

Kip1 is required for robust CPC midzone localization

To determine whether any of the nuclear kinesins might recruit the CPC to the spindle midzone, we analyzed CPC localization in mutants of each of these nuclear kinesins. We looked specifically at cells expressing Nbl1-GFP to follow the CPC and mCherry-Tub1 to show the spindle in strains with *kip1Δ*, *cin8Δ*, or *kip3Δ* mutations. We imaged live cells using a mixed population of WT and mutant strains in each sample to compare fluorescence intensities directly. To distinguish between WT and mutant strains, the WT strain also expressed the spindle pole body protein Spc42 labeled with mCherry in addition to Nbl1-GFP and mCherry-Tub1 (Fig. 2 H). To quantify accurately any difference in the amount of CPC at the midzone in WT and mutant strains, we analyzed Nbl1-GFP fluorescence intensity over a span of 4 µm at the midzone. We then quantified the area under the peak for each of the graphs. To ensure that the mCherry tag on Spc42 did not affect our quantification, we compared the localization of the Nbl1-GFP in WT strains expressing either mCherry-Tub1 alone or mCherry-Tub1 and Spc42-mCherry. The CPC was able to concentrate at the midzone to the same extent in both WT strains, indicating that the Spc42-mCherry marker did not affect our quantification (Fig. 2, A and I). Deletion of *CIN8* did not have any detectable effect on CPC localization at the midzone (Fig. 2, B and I). Strikingly, deletion of *KIP1* decreased CPC midzone localization by 53% (Fig. 2, C and I). Deletion of *KIP3* decreased the amount of CPC at the midzone by 23%. However, the latter difference was not statistically significant (Fig. 2, D and I). All of the strains analyzed expressed the same levels of Nbl1-GFP as demonstrated by Western blot analysis (Fig. S1). At this point, our results indicate that Kip1 is required for efficient localization of the CPC to the spindle midzone.

Kip1 and Cin8 are required to drive spindle elongation during anaphase B

Despite the striking reduction in the amount of CPC at the spindle midzone in *kip1Δ* cells, some CPC was still concentrated in the midzone in the absence of Kip1. Cin8 and Kip1 are known to have partially overlapping functions (Hoyt et al., 1992). Therefore, we hypothesized that Cin8 might be able to provide some Kip1 function during late anaphase if Kip1 is absent. This would explain why the CPC is partially localized to the spindle midzone in a Kip1 null strain. To address this possibility, we generated a strain deficient in both *KIP1* and *CIN8*. Because the presence of at least one of the motors is essential for viability, we created an auxin-inducible degron (AID) mutant (Nishimura et al., 2009; Morawska and Ulrich, 2013) of Cin8 (CIN8-AID*) that allows rapid Cin8 degradation upon addition of auxin to the growth medium and combined it with a *kip1Δ* mutation. A *kip1Δ* CIN8-AID* strain expressing the ubiquitin ligase TIR1 died in medium containing auxin, whereas the strain survived if it did not express TIR1, indicating that the degron is functional (Fig. 2 G). Immunoblotting confirmed that Cin8 is reduced to almost undetectable levels upon treatment with 250 µM auxin for 15 min (Fig. S2). To determine how the absence of both motors affects CPC midzone localization during anaphase, *kip1Δ* CIN8-AID* cells expressing Nbl1-GFP and mCherry-Tub1 were arrested with α factor, released into imaging medium, and observed until they entered anaphase, at which

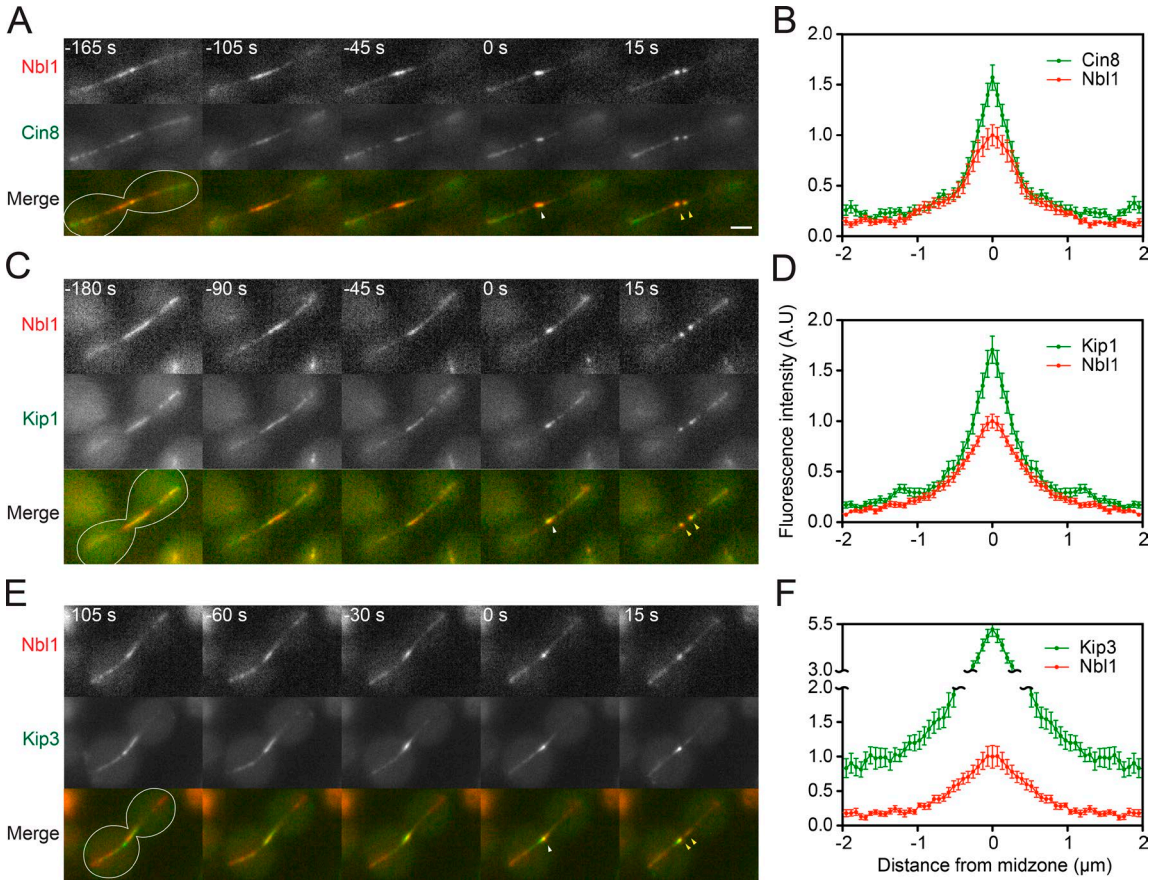

Figure 1. **The CPC colocalizes with Kip1, Cin8, and Kip3 at the spindle midzone in late anaphase. (A, C, and E)** Time lapse of yeast cells expressing Nbl1-mCherry (top rows) as well as Cin8-GFP, Kip1-GFP, or Kip3-GFP (middle rows). The merged image of Nbl1-mCherry (red) and Cin8-GFP, Kip1-GFP, or Kip3-GFP (green) is shown on the bottom row of each panel. Cells are undergoing late anaphase and spindle disassembly. Time in seconds is shown on the top right corner. t = 0 represents the time just before the spindle is broken and is the frame used for the quantification shown on the right of each panel. White arrowheads indicate positions of the spindle midzone. Yellow arrowheads point to the ends of shrinking microtubules in the disassembling half spindles. Cell outlines are shown in white. Bar, 2 µm. **(B, D, and F)** Graphs show normalized fluorescence intensity versus distance from the spindle midzone (0 µm) on the frame just before the onset of spindle disassembly. Each graph compares the position of the fluorescence intensity peak of Nbl1 (red) with the position of the fluorescence intensity peak of each kinesin (green; B: Cin8, n = 9; D: Kip1, n = 13; F: Kip3, n = 10). Error bars represent SEM.

point 250 µM auxin was added to the medium. We noticed that WT spindles reached full anaphase length ∼1.5 h after release from α factor and started disassembly when they reached a length of 9.4 ± 0.1 µm. In contrast, 1.5 h after release from α factor, *kip1Δ CIN8-AID** spindles that had been treated with auxin did not reach full anaphase length. Most of these cells were large budded and had short spindles that broke prematurely at a mean length of 7.0 ± 0.7 µm (Fig. S2). The fact that all short spindles eventually break without completing anaphase is consistent with the spindle being sheared by contraction of the actomyosin ring or cytokinesis itself. This result indicates that cells still progress into cytokinesis even though they have not yet completed anaphase. Previous studies have shown that Cin8 and Kip1 play a role during anaphase B (Straight et al., 1998; Movshovich et al., 2008). Our results, however, demonstrate that their activity is essential for anaphase spindle elongation.

To determine whether Cin8 and Kip1 have partially overlapping functions to recruit the CPC to the midzone in late anaphase, it was necessary to fully elongate the spindle in the absence of both motors. The structure of the mitotic spindle is maintained by counteracting forces generated by Cin8/Kip1, dynein, and Kar3 (Saunders and Hoyt, 1992; Saunders et al., 1995). Previous studies showed that deletion of *KAR3* suppresses the temperature sensitivity of a *cin8-3 kip1Δ* strain (Saunders and Hoyt, 1992; Hoyt et al., 1993). This is because dynein provides sufficient pulling force to elongate the spindle when Kar3 is not present (Cottingham et al., 1999). Similarly, deletion of *KAR3* in the *kip1Δ CIN8-AID** strain partially rescued the lethality of this double mutant (Fig. 2 G). Deletion of *KAR3* also rescued the short spindle phenotype, as the mean spindle length before spindle breakdown in the triple-mutant *kip1Δ kar3Δ CIN8-AID** was 8.8 ± 0.3 µm and not statistically different from the mean WT spindle length (Fig. S2). These results are consistent with findings by Saunders and Hoyt (1992) and Saunders et al. (1995) and show, using live-cell analysis, that Kip1 and Cin8 are essential not only to separate spindle poles but also for anaphase progression.

Neither Cin8 nor Kar3 is required to concentrate the CPC at the midzone

In WT cells, the CPC concentrates at the midzone just before the spindle breaks and then follows the depolymerizing ends of microtubules (Fig. 1; Nakajima et al., 2009). However, in *kip1Δ*

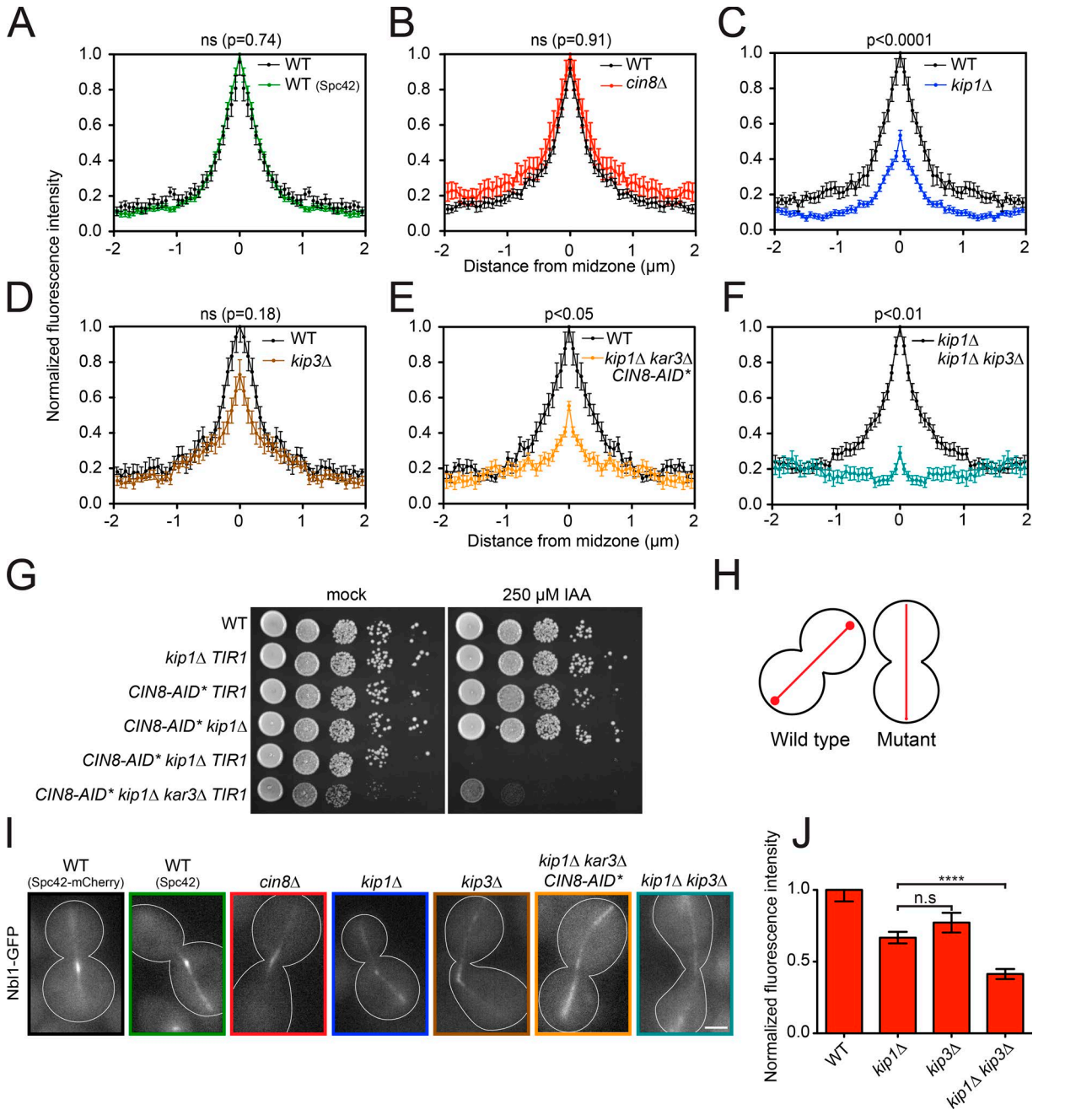

Figure 2. **The CPC cannot concentrate at the spindle midzone in the absence of Kip1 and Kip3. (A–F)** Graphs show normalized fluorescence intensity versus distance from the spindle midzone (0 µm) on the frame just before the onset of spindle disassembly for WT (black line) and each of the mutants or WT control (varying colors). The number of cells analyzed for each graph were (black/color): 15/30 (A), 16/13 (B), 11/23 (C), 6/8 (D), 10/10 (E), and 15/8 (F). **(G)** Growth assay to assess the viability of the *kip1Δ CIN8-AID** strain. Five different dilutions of each strain were pipetted onto two types of YPD plates: mock (YPD + DMSO) and YPD + 250 µM IAA. The assay shows that degradation of Cin8 is dependent on TIR1 and that the lethality caused by Cin8 degradation in *kip1Δ* cells can be partially rescued by additionally deleting *KAR3*. **(H)** Schematic of the experimental design. To be able to compare fluorescence intensities of WT and mutant strains, the strains were mixed and observed on the same coverglass. Both WT cells and mutants expressed Nbl1-GFP and mCherry-Tub1, but WT cells also expressed Spc42-mCherry, which allowed us to distinguish the WT cells from the mutants when they were cocultured. **(I)** Fluorescence images of representative cells just before the onset of spindle disassembly that are expressing Nbl1-GFP and carrying the indicated mutation. Cell outlines are shown in white. Bar, 2 µm. **(J)** Graph shows relative fluorescence intensity along the entire length of the spindle for each of the strains noted and normalized to WT cells. *n* = 17 (WT), 28 (*kip1Δ*), 15 (*kip3Δ*), and 18 (*kip1Δ kip3Δ*). Error bars represent SEM; ****, P ≤ 0.0001.

*CIN8-AID** cells, the CPC evenly decorates the entire length of the short anaphase spindles and is not concentrated at the midzone at the time the spindle breaks (Fig. S2). At least two possible explanations exist for why the CPC is not recruited to the midzone. One possibility is that it cannot get to that region because both Kip1 and Cin8 are required to transport it there. Another possibility is that a structure or signaling event required for this process is only present in long anaphase spindles and not

in the early anaphase spindles of the double mutant. To distinguish between these possibilities, we analyzed CPC localization on long anaphase spindles of the triple *kip1Δ kar3Δ CIN8-AID** mutant. Analysis of GFP fluorescence intensity on long anaphase spindles of the triple *kip1Δ kar3Δ CIN8-AID** mutant revealed that the CPC was able to localize to the midzone of these cells to a similar extent as in *kip1Δ* single mutants (Fig. 2, E and I). This result demonstrates that Cin8 and Kar3 are not required to concentrate the CPC at the spindle midzone and suggests that an additional mechanism partially recruits it to that region in the absence of Kip1.

CPC localization at the spindle midzone is dependent on Kip1 and Kip3

Even in the absence of three of the four nuclear kinesins, some Nbl1 was able to concentrate at the spindle midzone in late anaphase. The only kinesin remaining was Kip3. Strikingly, when we knocked out both Kip1 and Kip3, the midzone localization of Nbl1-GFP was completely abolished (Fig. 2, F and I). Previous research has shown that there are discrete Aurora B–Ipl1 passenger complexes that do not contain all four subunits and that these subcomplexes have specific functions during anaphase (Thomas and Kaplan, 2007). To determine whether the observed mislocalization of Nbl1 also affects other subunits of the CPC, we looked at the localization of Sli15 in the *kip1Δ kip3Δ* double mutant and the *kip1Δ* single mutant. As for Nbl1, the midzone localization of Sli15 was completely abolished in the double mutant (Fig. S2).

We considered the possibility that the inability of the CPC to concentrate at the spindle midzone might be an indirect consequence of midzone defects caused by the absence of the two motors. To address this possibility and to determine whether this defect also affects other midzone proteins, we analyzed the localization of two well-characterized midzone proteins, Bim1 and Ase1, in cells lacking both Kip1 and Kip3. In WT cells, Bim1 localizes to the spindle midzone of anaphase cells; then, it gradually dissociates as the cell progresses through anaphase, and a small amount of Bim1 remains at the midzone and tracks the depolymerizing ends of the spindle microtubules upon spindle breakage (Fig. 3 A; Zimniak et al., 2009). Quantification revealed that 94.6% of WT cells (n = 37) had visible Bim1 remaining at the spindle midzone. Strikingly, in the *kip1Δ kip3Δ* double mutant where the CPC is unable to concentrate at the midzone, Bim1 still localized to that region during anaphase, and 93.2% of *kip1Δ kip3Δ* cells (n = 44) had Bim1 remaining at the spindle midzone at the onset of spindle disassembly (Fig. 3 B). The same was true for Ase1, which localizes to and stabilizes the spindle midzone throughout mitosis (Khmelinskii and Schiebel, 2008). We observed Ase1 localization to the spindle midzone just before the onset of spindle disassembly in 100% of WT cells (n = 91; Fig. 3 C) and in 97.6% of *kip1Δ kip3Δ* cells (Fig. 3 D). Although CPC midzone localization was completely abolished in *kip1Δ kip3Δ* cells (Fig. 2, F and I), both Bim1 and Ase1 had a robust midzone localization in this double mutant (Fig. 3, B and D). Collectively, these results, which show that that two major midzone proteins are able to localize to the spindle midzone of *kip1Δ kip3Δ* cells, demonstrate that there is a functional spindle midzone in double *kip1Δ kip3Δ* mutants and indicate that there is a direct relationship between the presence of Kip1 and Kip3 and the recruitment of the CPC to the spindle midzone.

To further analyze the role of Kip1 and Kip3 in CPC midzone localization, we determined whether the lack of CPC enrichment at the midzone was compensated by a higher amount of CPC along the entire spindle. This would suggest that the motors are responsible for transporting the CPC to the midzone. Analysis of Nbl-GFP fluorescence along the entire length of the spindle for WT cells and for each of the mutants that showed some degree of defect revealed that in the absence of either Kip1 or Kip3, the amount of Nbl1 on the spindle is reduced by 33% or 23%, respectively. In the double *kip1Δ kip3Δ* mutant, the amount of Nbl1 on the spindle was reduced by 59%, suggesting an additive effect of Kip1 and Kip3 (Fig. 2 J). These data indicate that Kip1 and Kip3 are only partially required for CPC binding to spindle microtubules.

CPC midzone localization is required for timely spindle disassembly

Previously, the budding yeast Aurora B CPC subunit Ipl1 was shown to be involved in spindle disassembly (Buvelot et al., 2003; Woodruff et al., 2010). To determine whether CPC midzone localization is required for efficient spindle breakdown, we analyzed this process in *kip1Δ kip3Δ* cells where the CPC is still active but unable to localize correctly to the midzone. We used Myo1-EGFP to follow contraction of the actomyosin cytokinetic ring and GFP-Tub1 to determine when the spindle breaks relative to when the actomyosin ring starts to constrict. We quantified the timing of spindle disassembly by measuring the diameter of the actomyosin ring at the time when the spindle breaks (D_b) and dividing this number by the diameter of the ring before it started to constrict (D_i; Fig. 4 G). In WT cells, the spindle breaks before the actomyosin ring has finished constriction. The same relative timing was observed in *kip1Δ* single mutants (Fig. 4, A and B). As previously observed (Woodruff et al., 2010), *kip3Δ* mutants exhibit delayed spindle disassembly as the spindle breaks only when the actomyosin ring has almost finished contraction (Fig. 4 C). Strikingly, the spindle of *kip1Δ kip3Δ* double mutants remains unbroken long after the actomyosin ring has contracted (Fig. 4 D), indicating that the spindle is more stable in the double mutant. These results show that both Kip1 and Kip3 are required for timely spindle disassembly and suggest that the spindle disassembly defect caused by their absence could be a consequence of the CPC not being able to concentrate at the spindle midzone to phosphorylate its targets, such as Bim1, to destabilize the midzone.

Zimniak et al. (2009) demonstrated that Bim1 phosphorylation by Ipl1 is required for efficient spindle disassembly. They showed that a Bim1^{6A} mutant that cannot be phosphorylated by Ipl1 fails to be removed from the spindle midzone during late anaphase and that the spindle does not disassemble efficiently. We wondered whether the spindle disassembly delay we observed in *kip1Δ kip3Δ* cells was solely a consequence of a failure to phosphorylate Bim1 and remove it from the midzone. To test this hypothesis, we mutated the six Ipl1 phosphorylation sites to mimic Ipl1 phosphorylation (Bim1^{6D}) and determined whether this phosphomimetic mutant could rescue the disassembly delay observed in *kip1Δ kip3Δ* cells. Quantification of spindle breakage relative to contraction of the cytokinetic ring revealed that there

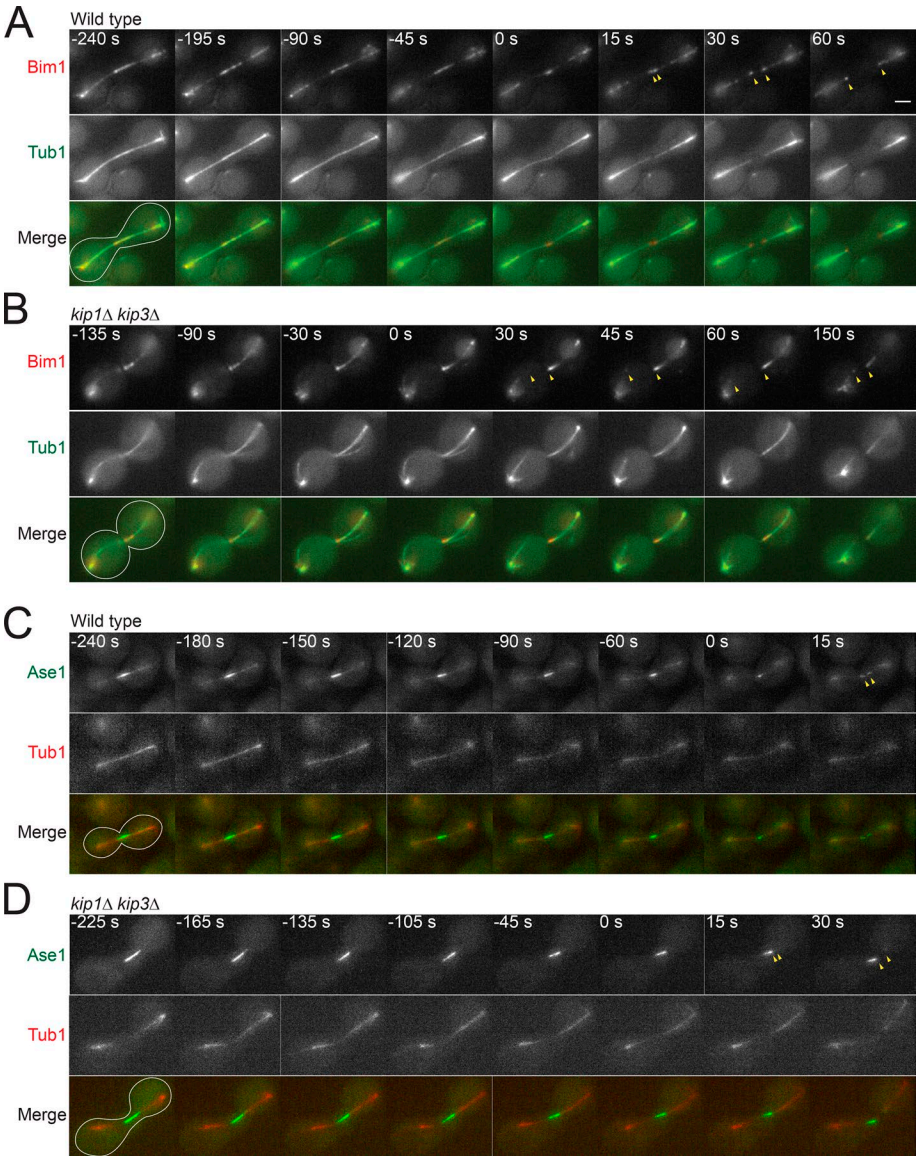

Figure 3. **Presence of a functional spindle midzone structure in the absence of both Kip1 and Kip3. (A–D)** Time lapse of WT (A and C) or *kip1Δ kip3Δ* (B and D) cells expressing either Bim1-tagRFPt and GFP-Tub1 (A and B) or Ase1-4GFP mCherry-Tub1 (C and D). Both Bim1 and Ase1 are prominently localized to the spindle midzone of WT and *kip1Δ kip3Δ* cells. Cells were arrested with α factor, released, and then imaged from late anaphase through spindle disassembly. Yellow arrowheads indicate depolymerizing spindle ends. Time in seconds is shown in the top left corner. t = 0 represents the time frame just before the onset of spindle disassembly. Cell outlines are shown in white. Bar, 2 µm.

is no significant difference in the timing of spindle disassembly between *kip1Δ kip3Δ* and *kip1Δ kip3Δ Bim1*^{6D} cells (Fig. 4 F). This result suggests that Bim1 is not the only target of the CPC at the spindle midzone to promote spindle disassembly and is in agreement with results from Woodruff et al. (2010) showing that Ipl1 has to phosphorylate and activate the spindle-destabilizing protein She1 for efficient spindle disassembly. However, we cannot rule out the possibility that other mechanisms downstream of Kip1 and Kip3 possibly independent of the CPC might also be necessary for efficient spindle disassembly.

CPC midzone localization is not essential to inhibit abscission through the NoCut pathway

Together with Boi1 and Boi2, one of the functions of Ipl1 during late anaphase is to inhibit abscission in cells with midzone defects through the NoCut pathway. This pathway ensures that cytokinesis only proceeds once all the chromosomes have cleared the division plane (Norden et al., 2006). We wondered whether CPC midzone localization is required for this inhibition and whether the inability of the CPC to concentrate to the midzone in *kip1Δ kip3Δ* cells activates the NoCut pathway, causing the observed delay in spindle disassembly. To answer the first question, we analyzed Boi1 and Boi2 localization. In WT cells, Boi1 and Boi2 localize to the bud neck during anaphase and relocate into the nucleus after spindle breakdown to allow abscission. In cells with midzone defects that hold the NoCut pathway active, Boi1 and Boi2 remain at the bud neck and delay abscission. Ipl1 activity is required for the localization of Boi1 and Boi2 to the bud neck as these proteins remain in the nucleus for the whole cell cycle in *ipl1-321* cells (Norden et al., 2006). To determine whether the midzone localization of the CPC is required to regulate Boi1 and Boi2 localization, we observed their localization in *kip1Δ kip3Δ* mutants. In *kip1Δ kip3Δ* double mutants, the same Boi1 and Boi2 localization as in WT cells was observed, suggesting that CPC midzone localization is not essential for proper Boi1 and Boi2 localization (Fig. S3). As midzone defects are known to affect Boi1 and Boi2 localization, the fact that their localization remains unchanged from WT cells further suggests that

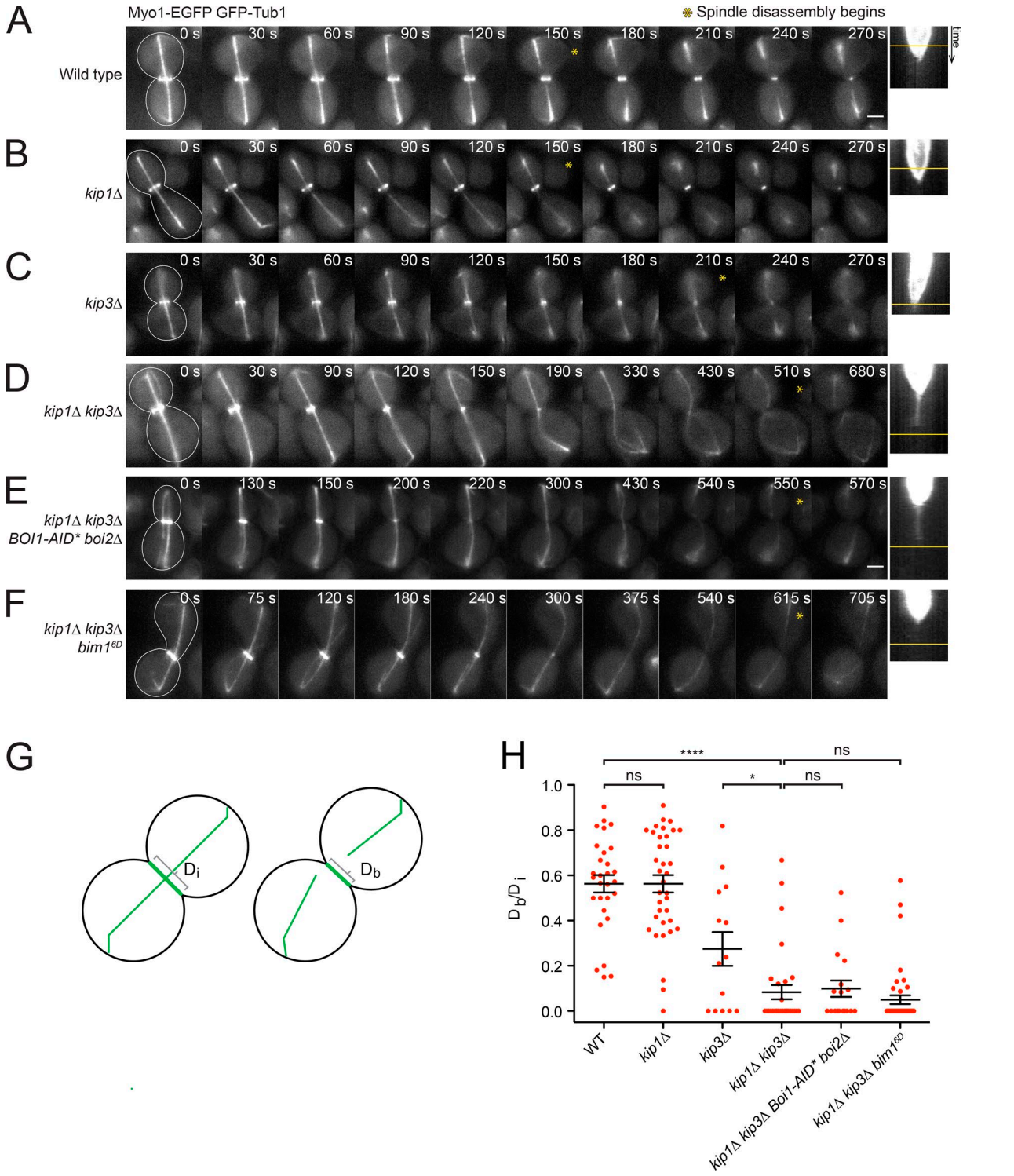

Figure 4. ***kip1Δ kip3Δ* cells exhibit severely delayed spindle disassembly. (A–F)** Time lapse of representative WT, *kip1Δ*, *kip3Δ*, *kip1Δ kip3Δ*, *kip1Δ kip3Δ Boi1-AID* boi2Δ*, and *kip1Δ kip3Δ* Bim1^{6D} cells expressing GFP-Tub1 and Myo1-GFP. Cells undergo anaphase followed by spindle disassembly. The yellow asterisk marks the point when the spindle breaks. Time in seconds is shown in the top right corner of each image, and t = 0 represents the frame around which the cytokinetic ring starts to contract. Cell outlines are shown in white. Bar, 2 µm. The corresponding kymograph showing contraction of the cytokinetic ring is shown to the right of each time-lapse series, with time on the y axis of the kymograph. On each kymograph, the yellow line indicates the frame in which the spindle breaks. **(G)** The cartoon represents a cell expressing Tub1-GFP and Myo1-GFP and shows the diameter of the ring before it has started to contract (D_i) and the diameter of the ring when the spindle breaks (D_b) to quantify the timing of spindle disassembly. **(H)** Quantification of D_b/D_i for each of the strains shown. n = 29 (WT), 36 (*kip1Δ*), 14 (*kip3Δ*), 31 (*kip1Δ kip3Δ*), 18 (*kip1Δ kip3Δ Boi1-AID* boi2Δ*), and 44 (*kip1Δ kip3Δ Bim1^{6D}*). Error bars represent SEM; *, P ≤ 0.05; ****, P ≤ 0.0001.

the midzone of *kip1Δ kip3Δ* cells is functional. Even though Boi1 and Boi2 localized normally in *kip1Δ kip3Δ* cells, we wondered whether the absence of the CPC at the midzone would hold the NoCut pathway active through a different mechanism and cause the observed delay in spindle disassembly. Deletion of *BOI1* and *BOI2* in cells with midzone defects that hold the NoCut pathway active was reported to rescue the abscission delay (Norden et al., 2006). In our strain background, double deletion of Boi1 and Boi2 was lethal. Therefore, we created an AID mutant of Boi1 (BOI1-AID*) and combined it with a *boi2Δ* mutation (Fig. S3). Depletion of Boi1 and Boi2 in the *kip1Δ kip3Δ* strain did not, however, rescue the delay in spindle disassembly (Fig. 4, E and H). Collectively, these data indicate that the spindle midzone in *kip1Δ kip3Δ* cells is unperturbed and suggest that CPC midzone localization is not essential for the early function of the NoCut pathway—namely, the relocalization of Boi1 and Boi2 to the bud neck. However, we cannot yet rule out the possibility that Ipl1 function could be required to delay abscission later in anaphase if there is incomplete clearance of chromatin from the spindle midzone.

Kip1 and Kip3 interact directly with the CPC and recruit it to microtubules in vitro

Our data demonstrate that Kip1 and Kip3 are required to localize the CPC to the spindle midzone. To determine whether they do this through a direct interaction or through an indirect mechanism, we analyzed purified proteins in vitro. We purified the four-subunit CPC labeled with a GFP tag on the Nbl1 subunit (CPC-GFP) and incubated it with microtubules in the presence or absence of unlabeled Kip1 or Kip3 that had been purified from budding yeast. We know that the CPC alone is able to bind microtubules with low affinity as we previously showed using a microtubule sedimentation assay (Kang et al., 2001; Cormier et al., 2013). As expected, however, at a low enough concentration, we did not observe any binding of CPC-GFP to microtubules (Fig. S4). Strikingly, in the presence of either Kip1 or Kip3, the amount of CPC-GFP bound was dramatically increased, indicating that Kip1 and Kip3 interact directly with the CPC and recruit it to microtubules (Fig. S4). These data are in agreement with our cell biology results showing that Kip1 and Kip3 are partially required for CPC binding to the mitotic spindle (Fig. 2 J). We repeated the experiment using Kip1-Halo purified from insect cells, which we found exhibits better motility in vitro than Kip1 purified from budding yeast, and used a higher concentration of CPC-GFP. At higher concentration, CPC-GFP alone could bind microtubules, and the amount of CPC-GFP bound increased over time (Fig. 5, A and B). However, in the presence of Kip1-Halo, CPC-GFP was able to bind microtubules faster and with higher efficiency (Fig. 5, A and B). These data confirm that Kip1 and Kip3 interact directly with the CPC and that they can recruit the CPC to microtubules.

The CPC diffuses on microtubules and is immobilized by Kip1

Our data show that the CPC interacts directly with Kip1 and Kip3, suggesting that the two kinesins recruit the CPC to the midzone in late anaphase through a direct interaction. At least two scenarios exist for how CPC recruitment to the midzone is achieved. In one scenario, the CPC is directly transported to the microtubule plus ends by the kinesins. In the other scenario, the CPC diffuses on microtubules and is trapped at the spindle midzone by association with Kip1 and Kip3. To distinguish between the two scenarios, we characterized the behavior of the CPC and Kip1 alone and together in single-molecule total internal reflection fluorescence (TIRF) experiments. We focused on the interaction between Kip1 and the CPC because our cell biology experiments indicated that Kip1 plays a more important role than does Kip3 in the recruitment of the CPC to the spindle midzone. Because Kip1-Halo purified from insect cells exhibited better motility than Kip1 purified from budding yeast, we performed the single-molecule experiments with Kip1-Halo. To increase the signal and to prevent photobleaching for single molecule tracking, we attached a quantum dot (QD) to Kip1-Halo and to the CPC. Quantum dots had been previously conjugated to anti-GFP antibodies to mediate their attachment to CPC-GFP (Xing et al., 2007). As previously reported (Fridman et al., 2013), Kip1-Halo exhibits bidirectional motility on microtubules in the presence of ATP (Fig. 5 C). Even though the motility is ATP dependent (Fridman et al., 2013), its bidirectional motility is well described by a diffusion model, with a diffusion coefficient of $1.704 \times 10^{-3} \pm 0.005 \times 10^{-3}$ $\mu m^2/s$ (Fig. 5 D). CPC-GFP alone diffuses on microtubules (Fig. 5 E), but it moves 100-fold faster than Kip1 (Fig. 5 G) and with a diffusion coefficient of 0.112 ± 0.0003 $\mu m^2/s$ (Fig. 5 F). To investigate the nature of their interaction, we looked at Kip1-Halo and CPC-GFP molecules together using dual-color TIRF. As indicated by their different diffusion coefficients, CPC-GFP moves much faster than Kip1 on the microtubule. When CPC-GFP encounters a Kip1 molecule, however, it stops diffusing (Fig. 5 H), with a binding time of 2.02 ± 0.04 s (Fig. 5 I). To determine whether the stop in CPC diffusion was caused by unspecific interaction with Kip1, we determined whether adding a different motor would have the same effect on CPC motility. For this quantification, we measured the percentage of freely diffusing CPC molecules without any motor or in the presence of either Kip1 or yeast dynein (Dyn1). Dyn1 binding to microtubules is sensitive to salt. Therefore, the experiment was performed without salt and also without ATP in order for Dyn1 to mimic the diffusion-like motility of Kip1. The CPC alone diffuses on microtubules, and it stops diffusing in the presence of Kip1. However, the diffusion of CPC was not affected by the presence of Dyn1, indicating that its interaction with Kip1 is specific. The motility of the CPC alone and CPC + Kip1 was not affected by the absence of salt and ATP (Fig. 5, J and K). Collectively, our data show that the interaction between CPC-GFP and Kip1 stops CPC-GFP diffusion and support a model in which the CPC is recruited to the spindle midzone by diffusing on the microtubule and then getting trapped by Kip1 once it reaches the spindle midzone. At this point, we cannot rule out the possibility that in the cell, there are additional factors or conditions that activate Kip1 to carry the CPC to the midzone actively.

Discussion

The CPC is a central regulator of distinct stages of mitosis, whose finely choreographed changes in localization underlie its ability to perform these functions. In this study, we focused on the mechanism by which the CPC relocalizes from the entire length of the spindle to the spindle midzone late in anaphase. A swift

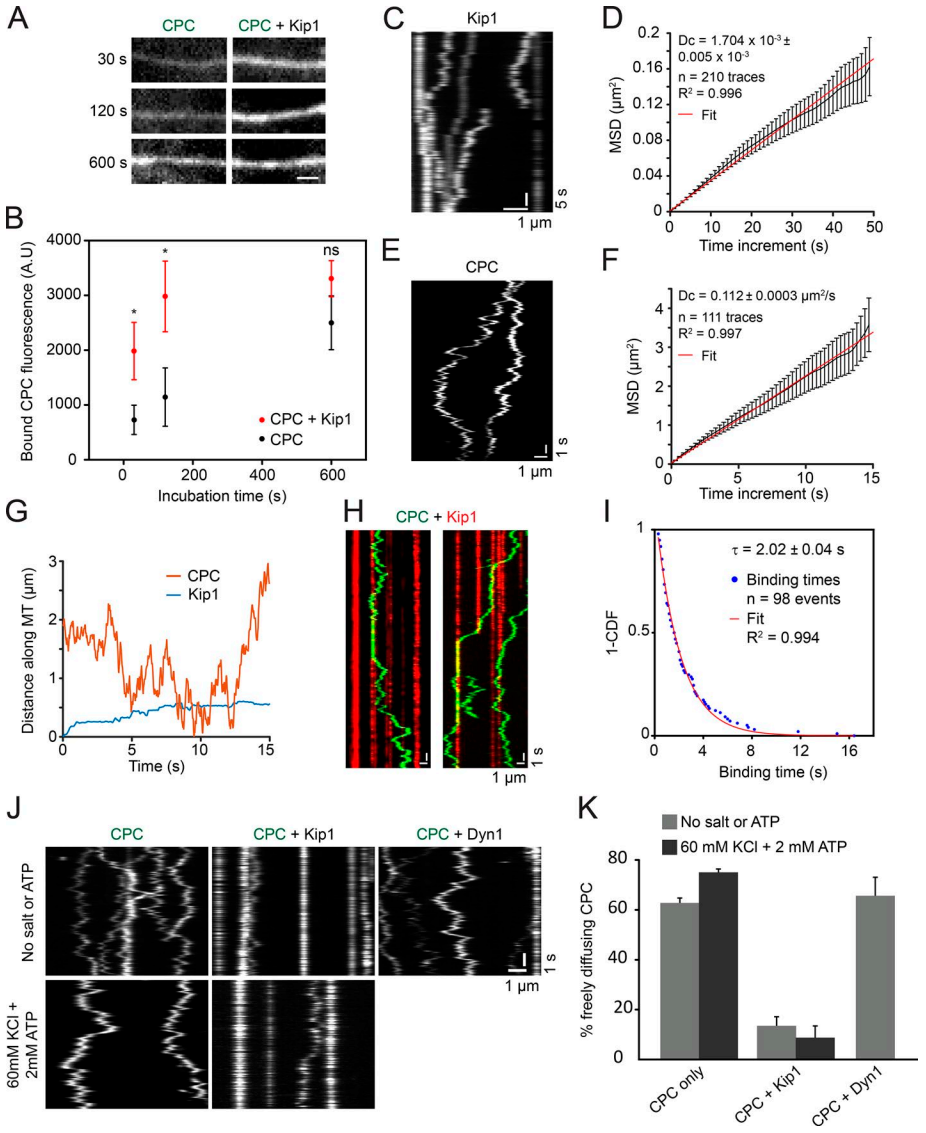

Figure 5. **Kip1 and Kip3 recruit the CPC to microtubules in vitro. (A)** Fluorescence images show purified CPC-GFP bound to axonemes in the absence (left) or presence (right) of unlabeled Kip1. Images in each condition were taken at the indicated time points. MB (see Materials and methods for composition) supplemented with 2 mM ATP and oxygen scavengers was used. Bar, 1 µm. **(B)** Graph showing bound CPC-GFP fluorescence on axonemes versus incubation time (means ± SD) in the presence or absence of Kip1 (red and white dots, respectively). *, P ≤ 0.05. **(C)** Representative kymograph showing Kip1-Halo motility on microtubules (MTs). Kip1-Halo was fluorescently labeled with a QD. **(D)** Graph showing MSD versus time increment for Kip1-Halo molecules. Diffusion coefficient and number of traces analyzed are indicated. **(E)** Representative kymograph showing CPC-GFP motility on microtubules. CPC-GFP was additionally labeled with a QD. Note the different time bar from the Kip1-Halo kymograph. **(F)** Graph showing MSD versus time increment for CPC-GFP molecules. Diffusion coefficient and number of traces analyzed are indicated. **(G)** Graph shows the distance traveled along the microtubule versus time for a single CPC-GFP molecule (orange) and for a single Kip1-Halo molecule (blue). **(H)** Representative dual-color kymographs showing the motility and interaction of CPC-GFP (green) and Kip1-Halo (red). **(I)** Graph shows 1-cumulative distribution function (1-CDF) versus binding times for 98 CPC-GFP::Kip1-Halo binding events. τ represents binding time between CPC-GFP and Kip1-Halo. **(J)** Representative kymographs of CPC-GFP motility alone (left), in the presence of unlabeled Kip1-Halo (middle), or in the presence of unlabeled Dyn1 (right). The two rows show two buffer conditions (MB + the indicated supplementation). **(K)** Bar graph showing the percentage of freely diffusing CPC molecules in each of the protein combinations indicated and in the two different buffers indicated. Error bars represent SEM.

change in localization presumably allows the CPC to regulate spindle disassembly. In mammalian cells, the kinesin 6 Mklp2 is required for the midzone localization of Aurora B (Gruneberg et al., 2004). However, neither the precise mechanism nor whether a direct physical interaction is involved has been determined. In this study, we combined yeast genetics with cell biology, biochemistry, and single-molecule microscopy to determine which of the nuclear kinesins, if any, are responsible for concentrating the CPC to the spindle midzone in yeast and to dissect the precise recruitment mechanism.

We systematically assessed the effect of deleting each of the nuclear plus end–directed kinesins, individually and in different combinations, on the amount of CPC present at the spindle midzone in late anaphase. We identified the kinesin 5 Kip1 and the kinesin 8 Kip3 as essential for the midzone localization of the CPC. In making combinatorial mutations of the kinesins to assess whether any is involved in or necessary for CPC localization to the midzone, we noticed that in the absence of both Kip1 and Cin8, spindles cannot fully elongate and break prematurely, indicating that both motors are required to elongate the spindle during anaphase. Saunders and Hoyt (1992) demonstrated that both Kip1 and Cin8 are essential to assemble and also maintain the spindle as metaphase spindles collapse in the absence of both motors. Straight et al. (1998) found that Cin8 and Kip1 have distinct roles during anaphase B: Cin8 is required for the rapid phase of anaphase B, and Kip1 activity is necessary for the slow phase of anaphase B (Straight et al., 1998). However, these observations did not reveal that the activity of either Kip1 or Cin8 is essential for anaphase progression. The AID system used in our study allowed us to rapidly deplete Cin8 from living cells, which enabled us to study the combined role of Kip1 and Cin8 during anaphase. Our study demonstrates that Kip1 and Cin8 are the main motors that promote spindle elongation during anaphase and

that dynein activity is not sufficient to counteract Kar3 pulling force during anaphase.

We showed that disassembly of the spindle is severely delayed in cells lacking both Kip1 and Kip3 and that the spindle breaks long after the cytokinetic ring has finished constriction. Kip1 has not previously been reported to be involved in spindle disassembly, and spindle disassembly is indistinguishable in WT and *kip1Δ* cells (Fig. 4, A, B, and H). Kip3, however, is a microtubule depolymerase believed to participate in spindle disassembly by actively depolymerizing spindle microtubules (Varga et al., 2006; Woodruff et al., 2010). Our data agree with conclusions from these earlier studies and additionally show that in *kip3Δ* mutants, spindle disassembly is delayed until the actomyosin ring has almost finished constriction (Fig. 4, C and H). The spindle disassembly delay in *kip3Δ* cells is, however, not as severe as in the double *kip1Δ kip3Δ* mutant (Fig. 4, D and H). The significantly longer delay in the double mutant is possibly the result of failure of the CPC to concentrate at the spindle midzone. However, we cannot rule out the possibility that other factors downstream of Kip1 and Kip3 and independent of the CPC might also be involved in spindle disassembly, and we note that Kip3's depolymerase activity is also likely to contribute to efficient spindle disassembly.

The Aurora kinase and CPC subunit Ipl1 has been shown previously to be involved in spindle disassembly (Buvelot et al., 2003; Woodruff et al., 2010). However, whether or not its midzone localization is required for this process was unclear. One of the targets of Ipl1 at the end of mitosis is Bim1, which is present at the spindle midzone and stabilizes the spindle until it dissociates from microtubules as the cell progresses through anaphase. A Bim1 mutant deficient in Ipl1 phosphorylation sites remains on the spindle midzone in late anaphase and delays spindle disassembly, suggesting that Ipl1 phosphorylates Bim1 at the midzone (Zimniak et al., 2009; Woodruff et al., 2010). We showed, however, that a Bim1 phosphomimicking mutant of the Ipl1 phosphorylation sites was not able to rescue the spindle disassembly delay in *kip1Δ kip3Δ* cells, suggesting that Bim1 is not the sole target of the CPC at the midzone to promote spindle disassembly. This result is in agreement with research from Woodruff et al. (2010) showing that Ipl1 needs to phosphorylate and activate the microtubule-destabilizing factor She1 for timely spindle disassembly.

We used an in vitro reconstitution assay to define the minimal number of components sufficient for efficient CPC microtubule association. As previously reported (Fridman et al., 2013), we also observed that Kip1 is a slow bidirectional motor. We found that the CPC alone can associate with microtubules, in agreement with our previous findings using a cosedimentation assay (Nakajima et al., 2011; Cormier et al., 2013). However, pure CPC did not associate with microtubule plus ends but associated along the entire microtubule length and diffused freely on the lattice. In contrast, when Kip1 was added to the assay, the CPC no longer diffused along microtubules but instead stopped diffusing when it encountered a Kip1 molecule. Based on its diffusion coefficient, it would take ∼90 s for a CPC molecule to diffuse from the far end of the spindle to the spindle midzone (∼4.5 µm). The CPC is, however, distributed over the entire length of the spindle, so it would take <90 s for most of the CPC to reach the midzone by simple diffusion, which fits with the timing observed in vivo. However, based on our results and results from other laboratories, Kip1 is slow and nonprocessive, which make it rather inefficient in reaching the microtubule end. We propose that rather than actively transporting the CPC, Kip1 and possibly Kip3 act as a trap at the midzone and capture diffusing CPC molecules, thereby concentrating them to that region and promoting efficient spindle disassembly. The CPC might diffuse along the spindle microtubules before being captured, or they might diffuse through the cytosol. What restricts this recruitment to late anaphase? Our previous work showed that a Sli15 mutant deficient in Ipl1 phosphorylation sites localizes prematurely to the midzone of early anaphase spindles. We therefore proposed that Sli15 dephosphorylation by Glc7/PP1, the phosphatase that opposes Ipl1, targets the CPC to the spindle midzone (Nakajima et al., 2011). Our current findings, collectively with previous research (Nakajima et al., 2011), suggest that Sli15 dephosphorylation mediated by Glc7/PP1 during late anaphase might trigger interaction of the CPC with Kip1 and Kip3 at the midzone, allowing CPC recruitment to that region.

The goal of this study was to gain a better understanding of how cells complete mitosis and accomplish spindle disassembly. We conclude that the action of two kinesins, Kip1 and Kip3, is essential to recruit the CPC to that region to promote efficient and timely spindle disassembly.

Materials and methods

Strain culture and construction

All yeast strains used in this study are S288c derivatives and are listed in Tables S1 and S2. Yeast were grown in yeast extract/peptone (YP) medium with 2% glucose (YPD) unless otherwise noted. To generate fluorescent protein fusions and gene deletions, we followed standard methods of PCR followed by yeast transformation and recombination (Longtine et al., 1998). To generate the AID strains, we used the plasmids described by Morawska and Ulrich (2013).

For the serial dilution assay, cells were grown overnight in YPD to saturation and diluted to OD_{600} 1 in YPD the next morning. We then made five sets of 10-fold dilutions and spotted 4 µl of each dilution onto agar plates. Cells were grown at the indicated temperatures for 48 h before being photographed.

Protein purification

CPC-GFP was purified essentially as reported for CPC by Cormier et al. (2013). For purification of Kip1 and Kip3 from budding yeast, plasmid pDD2667 or pDD2666, respectively, was transformed into the yeast strain D1074 (gift from D. D'Amours, University of Montreal, Montreal, Canada). Overnight-saturated precultures in synthetic minimal medium (yeast nitrogen base without amino acids) supplemented with 2% raffinose and dropout uracil and leucine were used to inoculate 2 liters of the same medium to OD_{600} 0.1 and were grown for 16 h at 30°C. Cultures were induced with 2% galactose for 9 h, harvested by centrifugation, drop frozen, and lysed using a 6870 Freezer/Mill (SPEX SamplePrep). Cell powder was thawed in 2× lysis buffer (Kip1: 100 mM NaH_2PO_4, pH 7.5, 1 M KCl, 1 mM ATP, 5 mM $MgCl_2$, 20 mM β-mercaptoethanol (BME), 2% Triton X-100, 20% glycerol, 80 mM imidazole, pH 7.5,

2 mM PMSF, and 2× cOmplete protease inhibitor cocktail without EDTA [Roche]; Kip3: 100 mM Hepes, pH 7.5, 1 M KCl, 1 mM ATP, 10 mM $MgCl_2$, 2 mM DTT, 2% Triton X-100, 20% glycerol, 80 mM imidazole, pH 8, 2 mM PMSF, and 2× cOmplete protease inhibitor cocktail without EDTA) and centrifuged for 30 min at 85,000 rpm in a TLA100.3 rotor (Beckman Coulter) at 4°C. Clarified lysate was injected into a HisTrap HP column (GE Healthcare), washed with wash buffer (Kip1: 50 mM NaH_2PO_4, pH 7.5, 500 mM KCl, 0.1 mM ATP, 1 mM $MgCl_2$, 10 mM BME, 1% Triton X-100, 10% glycerol, 40 mM imidazole, pH 7.5, 1 mM PMSF, and 1× cOmplete protease inhibitor cocktail without EDTA; Kip3: 50 mM Hepes, pH 7.5, 200 mM KCl, 0.5 mM ATP, 5 mM $MgCl_2$, 1 mM DTT, 1% Triton X-100, 10% glycerol, 40 mM imidazole, pH 8, 1 mM PMSF, and 2× cOmplete protease inhibitor cocktail without EDTA), and eluted with a buffer gradient going from wash buffer to elution buffer (Kip1: 50 mM NaH_2PO_4, pH 7.5, 250 mM KCl, 0.1 mM ATP, 1 mM $MgCl_2$, 10 mM BME, 10% glycerol, and 1 M imidazole, pH 7.5; Kip3: 50 mM Hepes, pH 7.5, 200 mM KCl, 0.5 mM ATP, 5 mM $MgCl_2$, 1 mM DTT, 1% Triton X-100, 10% glycerol, and 1 M imidazole, pH 8) over 20 min. Elution fractions containing Kip1 or Kip3 were pooled together, and the buffer of Kip1 was exchanged to final buffer (50 mM NaH_2PO_4, pH 7.5, 250 mM KCl, 0.1 mM ATP, 1 mM $MgCl_2$, 10 mM BME, and 20% glycerol) using a desalting column (PD10; GE Healthcare). At this step, Kip1 and Kip3 were incubated with 6×His-TEV protease overnight at 4°. The next morning, Kip1 containing 6×His-TEV was incubated with 500 µl of Ni-NTA agarose (Thermo Fisher Scientific) for 2 h at 4°C and centrifuged for 1 min at 1,000 *g* to separate the resin containing 6×His-TEV from the supernatant with Kip1. The supernatant was collected, concentrated using an Amicon centrifugal filter unit (EMD Millipore), aliquoted, and flash snapped in liquid N_2. Kip3 containing 6×His-TEV buffer was exchanged to low-salt buffer (50 mM Hepes, pH 7.5, 100 mM KCl, 0.5 mM ATP, 5 mM $MgCl_2$, 1 mM DTT, 1% Triton X-100, and 10% glycerol), and the protein was bound to a HisTrap Capto Q (GE Healthcare) and eluted using a buffer gradient going from low-salt buffer to high-salt buffer (50 mM Hepes, pH 7.5, 1 M KCl, 0.5 mM ATP, 5 mM $MgCl_2$, 1 mM DTT, 1% Triton X-100, and 10% glycerol) over 20 min. Kip3 and 6×TEV eluted at different salt concentrations. Elution fractions that contained Kip3 were pooled together, and the buffer was exchanged to final buffer (50 mM Hepes, pH 7.5, 200 mM KCl, 0.5 mM ATP, 5 mM $MgCl_2$, 1 mM DTT, 1% Triton X-100, and 10% glycerol) using a PD10 desalting column. The protein was concentrated with an Amicon centrifugal filter unit (EMD Millipore), aliquoted, and snap frozen in liquid N_2.

Kip1-Halo expression and purification from insect cells was adapted from Zhang et al. (2017). In brief, the Kip1 gene was cloned into a pOmniBac plasmid (64070; Addgene) to generate pDD2669. Bacmid was generated in DH10bac cells and transfected into Sf9 insect cells using Fugene (Promega). Virus was amplified to P2, and 5 ml was added to 1 liter Sf9 cells. After 3 d, cells were harvested by centrifugation, and the pellet was flash frozen. Cells were thawed in lysis buffer (50 mM Hepes, pH 7.4, 100 mM NaCl, 10% glycerol, 1 mM DTT, 0.1 mM ATP, and 2 mM PMSF) with one protease inhibitor tablet added per 50 ml (cOmplete EDTA-free protease inhibitor tablet) and lysed with a dounce. Lysate was centrifuged (503,000 rcf for 45 min at 4°C; Type 70 Ti rotor; Beckman Coulter) and bound to IgG Sepharose 6 Fast Flow beads (GE Healthcare) for 1 h. Beads were washed with lysis buffer and equilibrated with TEV buffer (50 mM Tris-HCl, pH 7.4, 150 mM KAc, 2 mM MgAc, 1 mM EGTA, 10% glycerol, 0.1 mM ATP, and 1 mM DTT). 100 µl of 4 mg/ml TEV protease was added and incubated overnight at 4°C. Amicon Ultracel concentrators (EMD Millipore) were used to concentrate the eluate. Protein was flash frozen in 10% glycerol. Yeast dynein was purified as described by Reck-Peterson et al. (2006).

Live-cell imaging

For live-cell microscopy, cells were grown to log phase at 25°C in imaging medium (Synthetic Complete medium lacking tryptophan and with 2% glucose) and immobilized on Concanavalin A–coated 25-mm round #1.5 coverslips. For imaging of cells during anaphase, cells were synchronized in G1 using α factor and released into imaging medium containing pronase. We followed the progression throughout mitosis by following the length of the spindle. About 1.5 h after release from α factor, ∼80% of the cells had reached anaphase, and this was when we started the imaging. For imaging of strains with an AID tag, 250 µM indolacetic acid (IAA) was added to the imaging medium 1.5 h after release from α factor. Imaging was started after 15 min of incubation with IAA. Videos were taken at 10- or 15-s intervals. Each frame of the video represents a maximum-intensity projection from a z stack containing three planes 0.4 µm apart. Images were processed using ImageJ software (National Institutes of Health).

Images were obtained using an Eclipse T*i* microscope (Nikon) controlled by MetaMorph (Molecular Devices) and equipped with a Plan Apochromat VC 100× 1.4 NA oil OFN25 differential interference contrast N2 objective, a MOV-2000 piezo stage (Applied Scientific Instrumentation), a Perfect Focus system (Nikon), a temperature-controlled enclosure (InVivo Scientific), and a Neo sCMOS camera (Andor Technology).

Time course and immunoblotting

To determine the timing of IAA-dependent Cin8-AID* and Boi1-AID* degradation, DDY5584, DDY5658, and DDY5655 precultures were diluted to OD_{600} 0.1 in imaging medium (Synthetic Complete medium lacking tryptophan and with 2% glucose) and grown to OD_{600} 0.5, at which point 250 µM IAA was added. An equal amount of cells was harvested for every time point during the 120-min time course. Cells were immediately precipitated with TCA as previously described (Foiani et al., 1994), and 0.5 OD_{600}s were loaded into each lane. The cell extracts were subjected to SDS-PAGE and immunoblot analysis using mouse anti-FLAG (Sigma-Aldrich) and mouse anti-Pgk1 (Invitrogen) antibodies.

Quantitative analysis of spindle fluorescence

The frame just before the spindle started to disassemble was identified from each video and adjusted to the same brightness and contrast parameters. We traced a segmented line along the entire length of the spindle to quantify the fluorescence intensity values of each pixel. The same line was moved parallel to the spindle to quantify background fluorescence and subtract it from the values of the spindle. The values were then corrected for photobleaching based on the frame of the video in which the spindle began

to disassemble. For the colocalization analysis of Nbl1 with each kinesin, we first identified the brightest pixel for each kinesin. Then, to prevent any bias based on the orientation of the spindle, we made the values of each spindle symmetric by inverting the intensity values of each spindle, aligning them at that pixel, and averaging them. Next, we identified the equivalent pixel in the Nb1 channel and again made the values for that channel symmetric around that pixel. We then aligned all the spindles in each channel around their symmetry point and averaged them to get the final value for the graph. To quantify the fluorescence intensity of Nbl1-GFP or Sli15-EGFP on the midzone, we first identified the midzone by finding in the mCherry-Tub1 channel the point where the spindle broke and then finding the equivalent pixel in the GFP channel. Next, we made the fluorescence intensity values for each spindle symmetric as mentioned above. All spindles were then aligned at the pixel where each spindle broke, and the values of all spindles were averaged. Experiments were repeated at least two times and quantified independently. Results from different days for a given combination of WT + mutant strains were similar. To quantify fluorescence intensity along the entire length of the spindle, we added the fluorescence values for each spindle and normalized them for the length of that spindle, and then we averaged all the normalized values for each strain.

In vitro TIRF binding assay

For the binding assay of CPC-GFP with Kip1 and Kip3 purified from budding yeast cells, coverslips and glass slides were cleaned with acetone and ethanol washes, and a flow chamber of ∼15 µl was constructed using double-sided tape. To block surfaces, 0.2% (wt/vol) Pluronic F127 (Invitrogen) in BRB80 (80 mM Pipes, pH 6.9, 1 mM EGTA, 1 mM $MgCl_2$, and 1 mg/ml casein) was flowed into the chamber and incubated for 10 min. Biotin-BSA (Vector Laboratories) at 5 mg/ml was flowed into the chamber, incubated for 10 min, and washed with BRB80, and then a 10-min incubation with 0.3 mg/ml Avidin DN (Vector Laboratories) was performed. The chamber was washed again with BRB80 and incubated with preassembled fluorescent microtubules. Microtubules were polymerized out of combination of unlabeled bovine tubulin, biotin-labeled tubulin (Cytoskeleton), and Cy3-labeled tubulin (labeled as described by Nicholas et al., 2014) and were stabilized with taxol. CPC-GFP was incubated with anti-GFP antibodies labeled with a QD (provided by A. Yildiz, University of California, Berkeley, Berkeley, CA) for 5 min, diluted to 1 nM in stepping buffer (80 mM Pipes, pH 6.9, 1 mM EGTA, 1 mM $MgCl_2$, 1 mg/ml casein, 0.01 µM taxol, 1 mM ATP, and glucose oxidase/catalase/dextrose) and then flowed into the flow chamber alone or in combination with 10 nM of Kip1, Kip3, or Kip1 + Kip3.

For the binding assay of CPC-GFP with Kip1-Halo purified from budding yeast cells, a flow chamber of ∼10 µl was constructed using double-sided tape, and sea urchin axonemes were immobilized on the glass coverslip (Cleary et al., 2014). Kip1 was diluted to 25 nM in motility buffer (MB; 30 mM Hepes, 5 mM $MgSO_4$, and 1 mM EGTA, pH 7.0, with KOH with 1 mg/ml casein and 1 mM tris(2-carboxyethyl)phosphine [TCEP]) and incubated for 10 min in the chamber containing the axonemes. Kip1 was washed out. CPC was diluted to 500 nM and incubated for stated periods of time. CPC was washed out and replaced with MB + 2 mM ATP + protocatechuic acid/protocatechuate-3,4-dioxygenase. GFP was imaged in TIRF with a 488-nm laser at 1.3 mW. Excitation was optimized so as to not saturate pixels at the highest CPC binding. All fluorescence quantifications were background subtracted. Experiments were repeated three times.

Kip1 and CPC single-molecule experiments

Halo-Tag ligand–labeled QDs were prepared by incubating amino-QDs (Q21521MP; Invitrogen) with Halo-Tag ligand *N*-hydroxysuccinimide ester (Promega). Anti-GFP antibody QDs were generated by linking TCEP-reduced antibody with amino-QDs via the heterobifunctional cross-linker sulfo-SMCC (Xing et al., 2007). Biotinylated microtubules were attached to glass coverslip using biotin-BSA and streptavidin. Kip1-Halo was labeled with 655-nm Halo-Tag ligand QDs. CPC-GFP was labeled with 655-nm-emission anti-GFP QDs. After binding QD-labeled Kip1 (50 pM) or CPC (500 pM) to the microtubule and washing, proteins were exchanged into MB (30 mM Hepes, 5 mM $MgSO_4$, 1 mM EGTA, pH 7.0, 1 mg/ml casein, and 1 mM TCEP) supplemented with 60 mM KCl, 2 mM ATP, and glucose oxidase/catalase/dextrose. Kip1 was imaged at 5 Hz, and CPC was imaged at 33 Hz. Experiments were repeated two times with $n > 100$ particles per experiment. For dual-color experiments, Kip1-Halo was labeled with 585-nm-emission Halo-Tag QDs, CPC-GFP was labeled with 655-nm-emission anti-GFP QDs, and MB buffer supplemented with 2 mM ATP, 60 mM KCl, and glucose oxidase/catalase/dextrose was used.

For the experiment containing CPC-GFP + dynein or Kip1, MTs were immobilized with biotin/streptavidin as described above. 10 nM nonfluorescent yeast dynein or Kip1 was flowed to the chamber after dilution in MB. After 2 min, excess protein was washed out. CPC-GFP was additionally labeled with anti-GFP QDs and diluted to single-molecule levels (<1 nM). After 2 min incubation of CPC-GFP, excess protein was washed out. Imaging was performed in the presence of 2 mM ATP, 60 mM KCl (or no salt/ATP as specified in figure), and gloxy/dextrose (oxygen scavenger). Oxygen scavengers were used with QDs to prevent blinking, not to prevent bleaching.

In vitro microscopy and analysis

Imaging was performed with a T*i*E Eclipse microscope (Nikon) with a 100× 1.49 NA Plan Apochromat TIRF objective and an Ixon electron-multiplying charge-coupled device camera (Andor Technology). Single-particle tracking was performed in MatLab (2015a; MathWorks) using Utrack software (Jaqaman et al., 2008). Mean square displacement (MSD) plots were generated using msdanalyzer (Tarantino et al., 2014). Plots of MSD versus time were fit to the equation $x^2 = 2Dt$. The means of the MSD values for all traces are plotted. Error bars represent SEM. Dual-color imaging was enabled by use of a W-View Gemini optosplit (Hamamatsu Photonics). Images were registered using Nile Red 0.5-µm beads (Spherotech) down to 43 ± 5 µm (1/2 pixel). Binding times were quantified using the measure function of ImageJ. Analysis of CPC-GFP and Kip-Halo binding time was performed as described in Chen et al. (2014).

Statistical analysis

For all statistical analyses, we used a two-tailed Student's *t* test in Prism (GraphPad Software).

Online supplemental material

Fig. S1 shows that Nbl1 colocalizes with spindle microtubules throughout anaphase and that Nbl1-GFP is expressed at the same levels in the strains used for microscopy. Fig. S2 shows the time course of auxin-dependent Cin8 degradation, a micrograph of the short spindle phenotype observed in the absence of both Kip1 and Cin8, a quantification of spindle length at the time of spindle disassembly in WT cells and different kinesin mutants, and a quantification showing that the defect in CPC midzone recruitment in the double *kip1Δ kip3Δ* is also true for Sli15. Fig. S3 shows a growth assay to assess the viability of a *kip1Δ kip3Δ boi2Δ BOI1-AID* strain and also shows that the localization of Boi1 and Boi2 is not affected in *kip1Δ kip3Δ* cells. Fig. S4 shows SDS-PAGE gels of the purified proteins used in the in vitro experiments, fluorescence images of purified CPC-GFP bound to microtubules in the presence or absence of either Kip1 or Kip3 purified from yeast, and a quantification of the amount of CPC-GFP bound to microtubules in each of the conditions. Table S1 lists all strains used in this study. Table S2 lists all plasmids used in this study.

Acknowledgments

We thank Jonathan Wong and Zane Bergman for critical reading of the manuscript, and we thank Michelle Lu, Matthew Akamatsu, Ross Pedersen, Nathaniel Krefman, Anthony Cormier, and all the members of the Barnes and Drubin laboratory for helpful discussions. We are grateful to Roberto Zoncu for help with TIRF microscopy and to Ahmet Yildiz, Doug Koshland, Isabelle Le Blanc, Jeremy Thorner, Larisa Gheber, and Damien D'Amours for sharing reagents.

This work was supported by a Boehringer Ingelheim Fonds PhD fellowship (to I. Ibarlucea-Benitez) and by the National Institutes of Health (grant R01 GM 47842 to G. Barnes).

The authors declare no competing financial interests.

Author contributions: I. Ibarlucea-Benitez, G. Barnes, and D.G. Drubin conceived and designed the experiments. I. Ibarlucea-Benitez and L.S. Ferro performed the experiments and analyzed the data. I. Ibarlucea-Benitez, G. Barnes, and D.G. Drubin wrote the manuscript.

Submitted: 17 August 2017
Revised: 30 January 2018
Accepted: 28 February 2018

References

Avunie-Masala, R., N. Movshovich, Y. Nissenkorn, A. Gerson-Gurwitz, V. Fridman, M. Kõivomägi, M. Loog, M.A. Hoyt, A. Zaritsky, and L. Gheber. 2011. Phospho-regulation of kinesin-5 during anaphase spindle elongation. *J. Cell Sci.* 124:873–878. https://doi.org/10.1242/jcs.077396

Buvelot, S., S.Y. Tatsutani, D. Vermaak, and S. Biggins. 2003. The budding yeast Ipl1/Aurora protein kinase regulates mitotic spindle disassembly. *J. Cell Biol.* 1:329–339.

Cheeseman, I.M., S. Anderson, M. Jwa, E.M. Green, J.-s. Kang, J.R. Yates III, C.S.M. Chan, D.G. Drubin, and G. Barnes. 2002. Phospho-regulation of kinetochore-microtubule attachments by the Aurora kinase Ipl1p. *Cell.* 111:163–172. https://doi.org/10.1016/S0092-8674(02)00973-X

Chen, J., Z. Zhang, L. Li, B.C. Chen, A. Revyakin, B. Hajj, W. Legant, M. Dahan, T. Lionnet, E. Betzig, et al. 2014. Single-molecule dynamics of enhanceosome assembly in embryonic stem cells. *Cell.* 156:1274–1285. https://doi.org/10.1016/j.cell.2014.01.062

Cleary, F.B., M.A. Dewitt, T. Bilyard, Z.M. Htet, V. Belyy, D.D. Chan, A.Y. Chang, and A. Yildiz. 2014. Tension on the linker gates the ATP-dependent release of dynein from microtubules. *Nat. Commun.* 5:4587. https://doi.org/10.1038/ncomms5587

Cormier, A., D.G. Drubin, and G. Barnes. 2013. Phosphorylation regulates kinase and microtubule binding activities of the budding yeast chromosomal passenger complex in vitro. *J. Biol. Chem.* 288:23203–23211. https://doi.org/10.1074/jbc.M113.491480

Cottingham, F.R., L. Gheber, D.L. Miller, and M.A. Hoyt. 1999. Novel roles for *saccharomyces cerevisiae* mitotic spindle motors. *J. Cell Biol.* 147:335–350. https://doi.org/10.1083/jcb.147.2.335

Foiani, M., F. Marini, D. Gamba, G. Lucchini, and P. Plevani. 1994. The B subunit of the DNA polymerase alpha-primase complex in *Saccharomyces cerevisiae* executes an essential function at the initial stage of DNA replication. *Mol. Cell. Biol.* 14:923–933. https://doi.org/10.1128/MCB.14.2.923

Fridman, V., A. Gerson-Gurwitz, O. Shapira, N. Movshovich, S. Lakämper, C.F. Schmidt, and L. Gheber. 2013. Kinesin-5 Kip1 is a bi-directional motor that stabilizes microtubules and tracks their plus-ends in vivo. *J. Cell Sci.* 126:4147–4159. https://doi.org/10.1242/jcs.125153

Gruneberg, U., R. Neef, R. Honda, E.A. Nigg, and F.A. Barr. 2004. Relocation of Aurora B from centromeres to the central spindle at the metaphase to anaphase transition requires MKlp2. *J. Cell Biol.* 166:167–172. https://doi.org/10.1083/jcb.200403084

Hoyt, M.A., L. He, K.K. Loo, and W.S. Saunders. 1992. Two Saccharomyces cerevisiae kinesin-related gene products required for mitotic spindle assembly. *J. Cell Biol.* 118:109–120. https://doi.org/10.1083/jcb.118.1.109

Hoyt, M.A., L. He, L. Totis, and W.S. Saunders. 1993. Loss of function of Saccharomyces cerevisiae kinesin-related CIN8 and KIP1 is suppressed by KAR3 motor domain mutations. *Genetics.* 135:35–44.

Hsu, J.Y., Z.W. Sun, X. Li, M. Reuben, K. Tatchell, D.K. Bishop, J.M. Grushcow, C.J. Brame, J.A. Caldwell, D.F. Hunt, et al. 2000. Mitotic phosphorylation of histone H3 is governed by Ipl1/aurora kinase and Glc7/PP1 phosphatase in budding yeast and nematodes. *Cell.* 102:279–291. https://doi.org/10.1016/S0092-8674(00)00034-9

Jaqaman, K., D. Loerke, M. Mettlen, H. Kuwata, S. Grinstein, S.L. Schmid, and G. Danuser. 2008. Robust single-particle tracking in live-cell time-lapse sequences. *Nat. Methods.* 5:695–702. https://doi.org/10.1038/nmeth.1237

Kang, J., I.M. Cheeseman, G. Kallstrom, S. Velmurugan, G. Barnes, and C.S. Chan. 2001. Functional cooperation of Dam1, Ipl1, and the inner centromere protein (INCENP)-related protein Sli15 during chromosome segregation. *J. Cell Biol.* 155:763–774. https://doi.org/10.1083/jcb.200105029

Khmelinskii, A., and E. Schiebel. 2008. Assembling the spindle midzone in the right place at the right time. *Cell Cycle.* 7:283–286. https://doi.org/10.4161/cc.7.3.5349

Kotwaliwale, C.V., S.B. Frei, B.M. Stern, and S. Biggins. 2007. A pathway containing the Ipl1/aurora protein kinase and the spindle midzone protein Ase1 regulates yeast spindle assembly. *Dev. Cell.* 13:433–445. https://doi.org/10.1016/j.devcel.2007.07.003

Longtine, M.S., A. McKenzie III, D.J. Demarini, N.G. Shah, A. Wach, A. Brachat, P. Philippsen, and J.R. Pringle. 1998. Additional modules for versatile and economical PCR-based gene deletion and modification in Saccharomyces cerevisiae. *Yeast.* 14:953–961. https://doi.org/10.1002/(SICI)1097-0061(199807)14:10%3C953::AID-YEA293%3E3.0.CO;2-U

Morawska, M., and H.D. Ulrich. 2013. An expanded tool kit for the auxin-inducible degron system in budding yeast. *Yeast.* 30:341–351. https://doi.org/10.1002/yea.2967

Movshovich, N., V. Fridman, A. Gerson-Gurwitz, I. Shumacher, I. Gertsberg, A. Fich, M.A. Hoyt, B. Katz, and L. Gheber. 2008. Slk19-dependent mid-anaphase pause in kinesin-5-mutated cells. *J. Cell Sci.* 121:2529–2539. https://doi.org/10.1242/jcs.022996

Murata-Hori, M., M. Tatsuka, and Y.L. Wang. 2002. Probing the dynamics and functions of aurora B kinase in living cells during mitosis and cytokinesis. *Mol. Biol. Cell.* 13:1099–1108. https://doi.org/10.1091/mbc.01-09-0467

Nakajima, Y., R.G. Tyers, C.C. Wong, J.R. Yates III, D.G. Drubin, and G. Barnes. 2009. Nbl1p: a Borealin/Dasra/CSC-1-like protein essential for Aurora/Ipl1 complex function and integrity in Saccharomyces cerevisiae. *Mol. Biol. Cell.* 20:1772–1784. https://doi.org/10.1091/mbc.E08-10-1011

Nakajima, Y., A. Cormier, R.G. Tyers, A. Pigula, Y. Peng, D.G. Drubin, and G. Barnes. 2011. Ipl1/Aurora-dependent phosphorylation of Sli15/INCENP regulates CPC-spindle interaction to ensure proper microtubule dynamics. *J. Cell Biol.* 194:137–153. https://doi.org/10.1083/jcb.201009137

Nicholas, M.P., L. Rao, and A. Gennerich. 2014. Covalent immobilization of microtubules on glass surfaces for molecular motor force measurements and other single-molecule assays. *Methods Mol. Biol.* 1136:137–169. https://doi.org/10.1007/978-1-4939-0329-0_9

Nishimura, K., T. Fukagawa, H. Takisawa, T. Kakimoto, and M. Kanemaki. 2009. An auxin-based degron system for the rapid depletion of proteins in nonplant cells. *Nat. Methods.* 6:917–922. https://doi.org/10.1038/nmeth.1401

Norden, C., M. Mendoza, J. Dobbelaere, C.V. Kotwaliwale, S. Biggins, and Y. Barral. 2006. The NoCut pathway links completion of cytokinesis to spindle midzone function to prevent chromosome breakage. *Cell.* 125:85–98. https://doi.org/10.1016/j.cell.2006.01.045

Petersen, J., J. Paris, M. Willer, M. Philippe, and I.M. Hagan. 2001. The S. pombe aurora-related kinase Ark1 associates with mitotic structures in a stage dependent manner and is required for chromosome segregation. *J. Cell Sci.* 114:4371–4384.

Reck-Peterson, S.L., A. Yildiz, A.P. Carter, A. Gennerich, N. Zhang, and R.D. Vale. 2006. Single-molecule analysis of dynein processivity and stepping behavior. *Cell.* 126:335–348. https://doi.org/10.1016/j.cell.2006.05.046

Saunders, W.S., and M.A. Hoyt. 1992. Kinesin-related proteins required for structural integrity of the mitotic spindle. *Cell.* 70:451–458. https://doi.org/10.1016/0092-8674(92)90169-D

Saunders, W.S., D. Koshland, D. Eshel, I.R. Gibbons, and M.A. Hoyt. 1995. *Saccharomyces cerevisiae* kinesin- and dynein-related proteins required for anaphase chromosome segregation. *J. Cell Biol.* 128:617–624. https://doi.org/10.1083/jcb.128.4.617

Shannon, K.B., and E.D. Salmon. 2002. Chromosome dynamics: new light on Aurora B kinase function. *Curr. Biol.* 12:R458–R460. https://doi.org/10.1016/S0960-9822(02)00945-4

Straight, A.F., J.W. Sedat, and A.W. Murray. 1998. Time-lapse microscopy reveals unique roles for kinesins during anaphase in budding yeast. *J. Cell Biol.* 143:687–694. https://doi.org/10.1083/jcb.143.3.687

Tarantino, N., J.Y. Tinevez, E.F. Crowell, B. Boisson, R. Henriques, M. Mhlanga, F. Agou, A. Israël, and E. Laplantine. 2014. TNF and IL-1 exhibit distinct ubiquitin requirements for inducing NEMO-IKK supramolecular structures. *J. Cell Biol.* 204:231–245. https://doi.org/10.1083/jcb.201307172

Thomas, S., and K.B. Kaplan. 2007. A Bir1p Sli15p kinetochore passenger complex regulates septin organization during anaphase. *Mol. Biol. Cell.* 18:3820–3834. https://doi.org/10.1091/mbc.E07-03-0201

Varga, V., J. Helenius, K. Tanaka, A.A. Hyman, T.U. Tanaka, and J. Howard. 2006. Yeast kinesin-8 depolymerizes microtubules in a length-dependent manner. *Nat. Cell Biol.* 8:957–962. https://doi.org/10.1038/ncb1462

Woodruff, J.B., D.G. Drubin, and G. Barnes. 2010. Mitotic spindle disassembly occurs via distinct subprocesses driven by the anaphase-promoting complex, Aurora B kinase, and kinesin-8. *J. Cell Biol.* 191:795–808. https://doi.org/10.1083/jcb.201006028

Woodruff, J.B., D.G. Drubin, and G. Barnes. 2012. Spindle assembly requires complete disassembly of spindle remnants from the previous cell cycle. *Mol. Biol. Cell.* 23:258–267. https://doi.org/10.1091/mbc.E11-08-0701

Xing, Y., Q. Chaudry, C. Shen, K.Y. Kong, H.E. Zhau, L.W. Chung, J.A. Petros, R.M. O'Regan, M.V. Yezhelyev, J.W. Simons, et al. 2007. Bioconjugated quantum dots for multiplexed and quantitative immunohistochemistry. *Nat. Protoc.* 2:1152–1165. https://doi.org/10.1038/nprot.2007.107

Zhang, K., H.E. Foster, A. Rondelet, S.E. Lacey, N. Bahi-Buisson, A.W. Bird, and A.P. Carter. 2017. Cryo-EM Reveals How Human Cytoplasmic Dynein Is Auto-inhibited and Activated. *Cell.* 169:1303–1314.e18. https://doi.org/10.1016/j.cell.2017.05.025

Zimniak, T., K. Stengl, K. Mechtler, and S. Westermann. 2009. Phosphoregulation of the budding yeast EB1 homologue Bim1p by Aurora/Ipl1p. *J. Cell Biol.* 186:379–391. https://doi.org/10.1083/jcb.200901036